An Electrochemical Model for Syngas Production by Co-electrolysis of H_2O and CO_2

Meng Ni*

Building Energy Research Group, Department of Building and Real Estate

The Hong Kong Polytechnic University, Hung Hom, Kowloon, Hong Kong, China

Abstract

Co-electrolysis of CO_2 and H_2O in a solid oxide electrolyzer cell (SOEC) offers a promising way for syngas production. In this study, an electrochemical model is developed to simulate the performance of an SOEC used for CO_2/H_2O co-electrolysis, considering the reversible water gas shift reaction (WGSR) in the cathode. The dusty gas model (DGM) is used to characterize the multi-component mass transport in the electrodes. The modeling results are compared with experimental data from the literature and good agreement is observed. Parametric simulations are performed to analyze the distributions of WGSR and gas composition in the electrode. A new method is proposed to quantify the contribution of WGSR to CO production by comparing the CO fluxes at the cathode-electrolyte interface and at the cathode surface. It is found that the reversible WGSR could contribute to CO production at a low operating potential but consume CO at a high operating potential. In addition, the contribution of WGSR to CO production also depends on the operating temperature and inlet gas composition.

Keywords:

Solid oxide fuel cell; Co-electrolysis; Synthetic fuel; Mass transfer; Porous media; Modeling

---

* Corresponding author. Tel: (852) 2766 4152; Fax: (852) 2764 5131;
Email: bsmengni@inet.polyu.edu.hk (Meng Ni)

1. Introduction

Hydrogen can be produced in a sustainable manner, such as by photocatalytic water splitting [1], gasification of biomass [2], solar thermochemical water-splitting [3], or water electrolysis driven by solar cells or wind turbines [4]. Among all the above technologies, water electrolysis is a practical and efficient method for large-scale hydrogen production. Alkaline electrolyzers and proton exchange membrane (PEM) electrolyzers usually work at room temperature. Solid oxide electrolyzer cells (SOECs) use the same materials with solid oxide fuel cells (SOFCs) but work in a reversed mode at a high temperature (i.e. 1073K). Compared with alkaline and PEM electrolyzers, SOECs consume less electricity as part of the energy needed for water splitting is in the form of heat [5]. Because of their great potential, SOECs have received increasing interest in recent years [6-20]. Various materials have been developed to fabricate SOEC for hydrogen production by steam electrolysis [21-23]. Several mathematical models have been developed to predict the SOEC performance at various levels [24-32].

In addition to steam electrolysis, SOECs can be used to electrolyze CO_2 for CO and O_2 production [33-39]. Co-electrolysis of CO_2 and H_2O has also been demonstrated to be feasible for simultaneous production of H_2 and CO [33-44], which can be subsequently processed for synthetic fuel production. In an SOEC used for H_2O/CO_2 co-electrolysis, 3 reactions take place simultaneously, namely H_2O electrolysis, CO_2 electrolysis, and reversible water gas shift reaction (WGSR). A common understanding on co-electrolysis is that the reversible WGSR should always contribute to CO production [38,40]. However, it is still not clear to which degree the reversible WGSR is responsible for CO production in the SOEC [45]. In addition, the existing studies on H_2O/CO_2 co-electrolysis are all experimental in nature, with aims to demonstrate the feasibility of this technology or to develop new materials for performance

improvement. The present literature is lacking detailed mathematical modeling of the SOEC used for H_2O/CO_2 co-electrolysis.

In this study, an isothermal electrochemical model is developed to characterize the performance of an SOEC used for CO_2/H_2O co-electrolysis. It is an extension of the previous models for CO_2 electrolysis and H_2O electrolysis, respectively [29, 46]. Both the co-electrolysis and the reversible WGSR inside the SOEC cathode are considered. The model is validated by comparing the simulation results with data from the literature. A new method is proposed to quantify the contribution of the reversible WGSR to CO production by comparing the fluxes of CO at the cathode-electrolyte interface and at the cathode surface. The results show that the reversible WGSR can produce or consume CO, depending on the average rate of WGSR in the cathode. This is different from the common understanding on H_2O/CO_2 co-electrolysis. The electrochemical model will be extended to 2D/3D model in a subsequent study.

2. Model development

2.1. Working principles

The working mechanisms of an SOEC for co-electrolysis of H_2O and CO_2 are shown in Figure 1. In the SOEC, the gas mixture of H_2O, CO_2, H_2, and CO flows in the cathode channel while air flows in the anode channel. In the porous cathode, both H_2O and CO_2 molecules diffuse through the porous electrode to the triple-phase-boundary (TPB) at the cathode-electrolyte interface, where they are reduced to H_2 and CO via reactions (1) and (2), respectively.

$$H_2O + 2e^- \rightarrow H_2 + O^{2-} \quad (1)$$

$$CO_2 + 2e^- \rightarrow CO + O^{2-} \quad (2)$$

The oxygen ions (O^{2-}) transport through the dense electrolyte to TPB at the electrolyte-anode interface, where they lose electrons to form oxygen molecules (Eq. 3). The produced oxygen molecules subsequently diffuse through the porous anode to the anode surface and get collected.

$$2O^{2-} \rightarrow O_2 + 4e^- \tag{3}$$

The overall reactions for H_2O electrolysis and CO_2 electrolysis can be written as,

$$H_2O \rightarrow H_2 + 0.5O_2 \tag{4}$$

$$CO_2 \rightarrow CO + 0.5O_2 \tag{5}$$

In addition to the above mentioned electrochemical reactions, reversible WGSR also occur in the cathode (Eq. 6).

$$H_2O + CO \rightleftarrows H_2 + CO_2 \tag{6}$$

In operation, the required potential (V) applied to SOEC can be expressed as,

$$V = E + \eta_{act,a} + \eta_{act,c} + \eta_{ohmic} \tag{7}$$

where E is the equilibrium potential (Nernst potential); η_{ohmic} is the ohmic overpotential; $\eta_{act,a}$ and $\eta_{act,c}$ are the activation overpotentials at the anode and cathode, respectively.

2.2. Equilibrium potentials including concentration overpotentials

The concentration overpotentials are not explicitly expressed in Eq. (7) as they are implicitly included in the Nernst potentials (Eqs. 8 and 9) for reactions (4) and (5), respectively [29,46],

$$E_{H_2} = E^0_{H_2} + \frac{RT}{2F} \ln \left[\frac{P^I_{H_2} \cdot \left(P^I_{O_2} \right)^{\frac{1}{2}}}{P^I_{H_2O}} \right] \tag{8}$$

$$E_{CO} = E_{CO}^{0} + \frac{RT}{2F} \ln \left[\frac{P_{CO}^{I} \cdot \left(P_{O_2}^{I} \right)^{\frac{1}{2}}}{P_{CO_2}^{I}} \right] \tag{9}$$

where E^0 is the voltage under standard conditions; $P_{H_2}^I$, $P_{H_2O}^I$, $P_{CO_2}^I$, P_{CO}^I and $P_{O_2}^I$ are the partial pressures of H_2, H_2O, CO_2, CO and O_2 at the electrolyte-electrode interface, respectively. T is temperature (K). R is the universal gas constant (8.3145 J.mol^{-1}K^{-1}); and F is the Faraday constant (96485 C.mol^{-1}). The E^0 can be calculated from thermodynamics ($\Delta G/(2F)$). At 600K and 1200K, the values of $E_{H_2}^0$ are 1.109017V and 0.940172V, respectively [47]. Similarly, the values of E_{CO}^0 are 1.195502V and 0.923869V, respectively. Assuming linear variation of E^0 between 600K and 1200K, the Nernst potentials (including concentration overpotentials) for Eqs. (4) and (5) can be written as,

$$E_{H_2} = 1.253 - 0.00024516T + \frac{RT}{2F} \ln \left[\frac{P_{H_2}^{I} \left(P_{O_2}^{I} \right)^{0.5}}{P_{H_2O}^{I}} \right] \tag{10}$$

$$E_{CO} = 1.46713 - 0.0004527T + \frac{RT}{2F} \ln \left[\frac{P_{CO}^{I} \left(P_{O_2}^{I} \right)^{0.5}}{P_{CO_2}^{I}} \right] \tag{11}$$

2.3. Multi-component mass transfer in porous electrodes

In order to determine the gas partial pressures at the electrolyte-electrode interface, the multi-component reactive-transport processes in the porous electrodes must be solved (Eq. 12). For modeling of multi-component reactive-transport in porous media, the Fick's Model (FM), Stefan-Maxwell Model (SMM), and the Dusty-Gas Model (DGM) have been widely used in the literature [48]. The DGM is used in the present study due to its better accuracy for multi-

component gas transport [49]. As the reversible WGSR does not change the total molar number of gas species, the pressure effect on mass transfer can be safely neglected [48, 50]. According to DGM, the reactive-transport of gas species *i* can be expressed as [49],

$$\frac{\varepsilon}{RT}\frac{\partial(y_i P)}{\partial t} = -\nabla N_i + R_i \tag{12}$$

$$\frac{N_i}{D_{i,k}^{eff}} + \sum_{j=1, j\neq i}^{n} \frac{y_j N_i - y_i N_j}{D_{ij}^{eff}} = -\frac{P}{RT}\frac{dy_i}{dx} \tag{13}$$

where y_i is the molar fraction of species *i*; ε is electrode porosity, R_i is the reaction rate (mol.m^{-3}.s^{-1}); $D_{i,k}^{eff}$ is the effective Knudsen diffusion coefficient (m^2.s^{-1}) of species *i*; D_{ij}^{eff} is the effective binary diffusion coefficient (m^2.s^{-1}) of species *i* and *j*; *P* is the pressure (Pa). N_i is the flux of species *i* (mol.m^{-2}.s^{-1}). d_c and d_a are thicknesses of cathode and anode, respectively. *x* is the depth inside the electrode, measured from the electrode surface, as can be seen from the computational domain shown in Fig. 1.

The effective binary diffusion coefficient (D_{ij}^{eff}) can be evaluated as,

$$D_{ij}^{eff} = \frac{\varepsilon}{\xi}\frac{0.0026T^{1.5}}{p\sqrt{M_{i,j}}\sigma_{i,j}^2\Omega_D} \tag{14}$$

$$M_{ij} = \frac{2}{\frac{1}{M_i} + \frac{1}{M_j}} \tag{15}$$

where ε/ξ is the ratio of porosity to tortuosity of porous electrodes; $\sigma_{i,j}$ is the mean characteristic length of species *i* and *j*; Ω_D is a dimensionless diffusion collision integral, which can be calculated as,

$$\sigma_{i,j} = \frac{\sigma_i + \sigma_j}{2} \tag{16}$$

$$\Omega_D = \frac{1.06036}{\tau^{0.1561}} + \frac{0.193}{\exp(0.47635\tau)} + \frac{1.03587}{\exp(1.52996\tau)} + \frac{1.76474}{3.89411\tau} \quad (17)$$

$$\tau = \frac{k_b T}{\varepsilon_{i,j}} \quad (18)$$

Here $k_b = 1.38066\times10^{-23}\left(\text{J.K}^{-1}\right)$ is the Boltzmann's constant. The values of σ_i and $\varepsilon_{i,j}$ can be used in the present study are summarized in Table 1 [51].

The Knudsen diffusion coefficient can be calculated as,

$$D_{i,k}^{eff} = \frac{\varepsilon}{\xi}\frac{2r_p}{3}\sqrt{\frac{8RT}{\pi M_i}} \quad (19)$$

where r_p is the radius of pores.

In the porous cathode, the transport of gas species is related to the rate of reversible WGSR and the rate of electrolysis reaction (current density). The rate (R_{WGSR}, $mol.m^{-3}.s^{-1}$) of reversible WGSR can be determined by a widely used formula as [52-59],

$$R_{WGSR} = k_{sf}\left(p_{H_2O}p_{CO} - \frac{p_{H_2}p_{CO_2}}{K_{ps}}\right) \quad (20)$$

$$k_{sf} = 0.0171\exp\left(\frac{-103191}{RT}\right) \qquad (mol.m^{-3}.Pa^{-2}.s^{-1}) \quad (21)$$

$$K_{ps} = \exp\left(-0.2935Z^3 + 0.6351Z^2 + 4.1788Z + 0.3169\right) \quad (22)$$

$$Z = \frac{1000}{T(K)} - 1 \quad (23)$$

The local mass conservation can be applied as,

$$\frac{dN_{H_2}}{dx} = R_{WGSR}\ ; \qquad \frac{dN_{H_2O}}{dx} = -R_{WGSR} \quad (24)$$

$$\frac{dN_{CO_2}}{dx} = R_{WGSR}\ ; \qquad \frac{dN_{CO}}{dx} = -R_{WGSR} \quad (25)$$

At the cathode-electrolyte interface, electrochemical reactions take place and thus the flux of H_2 and CO can be related to the current densities as,

$$N_{H_2}\Big|_{x=d_c} = -\frac{J_{H_2}}{2F}; \qquad N_{H_2O}\Big|_{x=d_c} = \frac{J_{H_2}}{2F} \tag{26}$$

$$N_{CO}\Big|_{x=d_c} = -\frac{J_{CO}}{2F}; \qquad N_{CO_2}\Big|_{x=d_c} = \frac{J_{CO}}{2F} \tag{27}$$

At the anode side, air is usually used as a sweep gas. The oxygen molecules produced at the TPB of anode transport to the anode surface and get collected. The flux of O_2 is related to the current density as,

$$N_{O_2}\Big|_{x=d_a} = -\frac{J_{CO} + J_{H_2}}{4F} \tag{28}$$

The above governing equations for describing the multi-component mass transfer are inter-related differential equations and can be solved by numerical method. The fourth order Runge-Kutta method is adopted for solving the DGM equations. After obtaining the partial pressure of gas species at the TPB (electrolyte-electrode interface), the Nernst potentials (including concentration overpotentials) can be calculated using Eqs. (10) and (11).

2.4. Activation overpotential

The activation overpotentials reflect the electrochemical activity of the electrodes. In the literature, the Butler-Volmer (BV) equation is the most widely adopted formula for describing the activation overpotentials of SOEC/SOFC. However, experimental works suggest that the activation overpotentials of SOEC/SOFC almost linearly vary with the current density [60]. In the present study, the linear formula is used [61].

$$\eta_{act,H_2,i} = \frac{RTJ_{H_2}}{n_{H_2}FJ^0_{H_2,i}} \tag{29}$$

$$\eta_{act,CO,i} = \frac{RTJ_{CO}}{n_{CO}FJ^0_{CO,i}} \tag{30}$$

where $J^0_{H_2,i}$ and $J^0_{CO,i}$ are the exchange current density for H_2O electrolysis and CO_2 electrolysis, respectively. The subscript i (i = a and c) represents the anode and cathode, respectively.

The exchange current densities ($J^0_{H_2,i}$ and $J^0_{CO,i}$) represent the readiness of the electrode to proceed with the electrochemical reaction and depend on the operating temperature as [62,63],

$$J^0_{H_2,c} = k_{H_2,c}\exp\left(-\frac{E_{act,c}}{RT}\right); \quad J^0_a = k_a\exp\left(-\frac{E_{act,a}}{RT}\right) \tag{31}$$

Here $k_{H_2,c}$ and k_a are the pre-exponential factors for the cathode (for H_2O electrolysis) and anode, respectively. The values of $E_{act,c}$ and $E_{act,a}$ are $1.0\times10^5 J.mol^{-1}$ and $1.2\times10^5 J.mol^{-1}$, respectively [62,63]. Chan et al. [64] recommend the values of $J^0_{H_2,c}$ and J^0_a at 1073K to be 5300 Am^{-2} and 2000 Am^{-2}, respectively. Using these values, the pre-exponential factors can be calculated. From experiments, the rate of electrochemical oxidation of H_2 is found about 2.5 times that of CO [65,66]. Thus, the exchange current density of the cathode for CO_2 electrolysis is calculated as $J^0_{CO,c} = 0.4J^0_{H_2,c}$.

2.5. Ohmic overpotential

As the interconnector and the electrodes have much higher electrical conductivity than the electrolyte, only the ohmic overpotential of SOEC electrolyte is considered in the present study. According to Ohm's law, the ohmic overpotential of the electrolyte can be calculated as [67],

$$\eta_{ohmic} = 2.99\times10^{-5} JL\exp\left(\frac{10300}{T}\right) \tag{32}$$

where L is the thickness of the electrolyte (m).

3. Results and Discussion

3.1. Model evaluation

In this section, the modeling results are compared with experimental data for model validation. In the literature, Zhan et al's work [36] on syngas production by co-electrolysis provides detailed experimental setup and operating conditions, such as the gas composition at the inlet and outlet, the thickness of the SOEC components, porosity of the electrodes, etc. In their study, the current density – voltage (J-V) characteristics of CO_2/H_2O co-electrolysis by a cathode-supported planar SOEC are measured. The thickness of Ni-YSZ (yttria-stabilized zirconia) cathode, LSCF-GDC (GDC: $Ce_{0.9}Gd_{0.1}O_{1.95}$; LSCF: $La_{0.6}Sr_{0.4}Co_{0.2}Fe_{0.8}O_3$) anode, and YSZ electrolyte are 600 μm, 20-30 μm, and 10 μm, respectively. The porosities of the cathode and anode are about 40% and 30%, respectively. At an operating temperature of 1073K, the molar fractions at the inlet of the cathode are: 50% H_2O, 25% H_2, and 25% CO_2. The current density and exhaust gas composition are measured at operating potentials from 0.95V to 1.3V. These operating conditions and structural parameters from the experiments [36] are used as input parameters in the theoretical simulation. Gas composition at the inlet, exhaust and the average of these two (should be more suitable) are used as gas composition at the cathode surface.

Figure 2 compares the modeling results with the experimental data from [36]. The difference between the modeling results and experimental data is smaller when the average gas composition is adopted. Although the calculated current density is about 25% smaller than the measured current density at 1.1V, the calculated data at other potentials agree well with the experimental results. In the subsequent parametric simulation, typical data from the literature

(i.e. thickness of SOEC components) are used, as shown in Table 2. It should be noted that there are 4 gas species in the cathode, although molar fractions of only 3 gas species are provided.

3.2. Effect of operating temperature

The effects of operating temperature on co-electrolysis of CO_2 and H_2O in an SOEC are shown in Fig. 3. It is found that the rate of reversible WGSR varies from negative values near the cathode surface to positive values near the cathode-electrolyte interface (Fig. 3a). The results also indicate that the WGSR does not reach equilibrium. The negative rate of WGSR at the cathode surface is mainly due to relatively high molar fractions of CO_2 and H_2 near the cathode surface (Figs. 3b and 3c). The positive rate of WGSR inside the cathode (particularly near the cathode-electrolyte interface) is mainly caused by relatively high concentration of CO inside the cathode (Fig. 3c). It is also found that the rate of WGSR increases with increasing temperature, due to the considerably increase in the value of k_{sf} from 1.14516×10^{-8} $mol.m^{-3}.Pa^{-2}.s^{-1}$ at 873K to 1.620625×10^{-7} $mol.m^{-3}.Pa^{-2}.s^{-1}$ at 1073K. The calculated rate of reversible WGSR is generally higher than the data for SOFC with internal reforming, such as [68]. This is because the rate of WGSR depends on not only the temperature, but also the products of p_{H_2O} and p_{CO} as well as p_{H_2} and p_{CO_2}, as can be seen from Eq. 19. The molar fractions of CO_2 and CO in an SOFC fueled by pre-reformed syngas are typically about 4.4% and 2.9%, respectively [52,68], much lower than the data used in SOEC for co-electrolysis. The current densities for H_2O electrolysis and CO_2 electrolysis increase with increasing temperature, as the activation overpotentials and the ohmic overpotential are smaller at higher temperature, (Fig. 3d).

A common understanding on co-electrolysis of H_2O/CO_2 in an SOEC is that the WGSR always contributes to CO production [38,40]. Based on existing experimental studies, it is difficult to confirm the above expectation and difficult to quantify the contribution of WGSR to

CO production [45]. It is understood that mass transfer becomes limiting only at very high current density and thus the CO production is governed by electrochemical reaction (electrolysis) and chemical reaction (WGSR). In this study, a new method is proposed to examine the contributions of reversible WGSR and electrolysis to CO production, by comparing the fluxes of CO at the cathode-electrolyte interface and at the cathode surface respectively. The flux of CO caused by electrochemical reaction can be easily calculated by Eq. (27). The difference in CO fluxes at the cathode surface and at the cathode-electrolyte interface is caused by the reversible WGSR. At a temperature of 873K, the fluxes of CO and H_2 are negative at the cathode surface. This means these species diffuse from the inside of the cathode to the cathode surface (Fig. 3e). Larger CO flux at the cathode surface than at the cathode-electrolyte interface (Eq. 27) means that the reversible WGSR contributes to CO production. The reversible WGSR and CO_2 electrolysis contribute to CO production by 25% and 75%, respectively (Fig. 3e). Accordingly, the reversed WGSR consumes H_2, leading to lower H_2 flux at the cathode surface than at the cathode-electrolyte interface (Fig. 3e). At 1073K, the CO flux at the cathode surface is about 19% lower than at the cathode-electrolyte interface (Fig. 3f), meaning that CO is consumed by WGSR. The above analyses show that the reversible WGSR can produce or consume CO, depending on the average rate of WGSR. It is also different from the common understanding on co-electrolysis that WGSR always contribute to CO production.

3.3. Effect of gas composition at the cathode surface

The inlet gas composition is varied to examine its effect on co-electrolysis behavior. Three cases are examined with different molar fractions at the cathode surface – case 1: H_2O (49.7%), H_2 (25%), CO_2 (25%), CO (0.3%); case 2: H_2O (49.7%), H_2 (0.3%), CO_2 (25%), CO

(25%); and case 3: H_2O (25%), H_2 (25%), CO_2 (49.7%), CO (0.3%). Figure 4a shows the comparison of the calculated rates of WGSR inside the porous cathode for the three cases, at operating temperature of 1073K, potential of 1.3V. It is found that the rate of WGSR is positive in most of the cathode layer for case 2 – decreasing from about 200 $mol.m^{-3}.s^{-1}$ at the cathode surface to about 0 at the cathode-electrolyte interface (Fig. 4a). For the other two cases (1 and 3) with very low CO molar fraction at the cathode surface, the rate of WGSR increases from negative values at the cathode surface to slightly positive values at the cathode-electrolyte interface. The molar fractions of gas species in the cathode for case 2 and 3 are shown in Figs. 4b and 4c. High molar fraction of CO is observed inside the cathode, indicating the slow diffusion of CO from the inside of the cathode to the surface of the cathode. For comparison, the light H_2 molecules can diffuse more easily thus the molar fraction variation is smaller. Despite the different rates of WGSR, there is no big difference in the calculated current density for different gas composition at the cathode surface (Fig. 4d). The fluxes of CO and H_2 are shown in Fig. 4e and 4f for case 2 and 3, respectively. For case 2, the CO flux increases from about $-0.02mol.m^{-2}.s^{-1}$ at the cathode-electrolyte interface to about $+0.02mol.m^{-2}.s^{-1}$ at the cathode surface (Fig. 4e). The negative flux at the electrode-electrolyte interface (E in Fig. 4e) represents CO production by electrochemical reaction (electrolysis). The positive flux at the cathode surface means that CO flows into the cathode, as WGSR consumes CO. Since H_2 is produced from reversible WGSR, the flux of H_2 at the cathode surface is higher than at the cathode-electrolyte interface. For case 3, the CO flux is considerably higher at the cathode surface than at the cathode-electrolyte interface (Fig. 4f), due to the high rate of the reversed WGSR inside the cathode.

3.4. Effect of applied potential

The effect of applied potential on co-electrolysis behavior of the SOEC is shown in Fig. 5. It is found that the rates of WGSR vary from about –200 $mol.m^{-3}.s^{-1}$ at the cathode surface to positive values at the cathode-electrolyte interface as the potential is increased from 1.0V to 1.4V (Fig. 5a). As expected, the current densities increase with increasing operating potential (Fig. 5d), which in turn increases the molar fraction of CO and H_2 inside the cathode (Fig. 5b, 5c). At a relatively low operating potential (1.0V), the CO flux at the cathode surface is about 3 times of the CO flux at the cathode-electrolyte interface (Fig. 5e), indicating the significant contribution of the reversed WGSR to CO production. In addition, the positive H_2 flux at the cathode surface means the H_2 molecules diffuse into the cathode and are consumed by the reversed WGSR (Fig. 5e). At an operating potential of 1.4V, the flux of CO at the cathode surface is smaller than at the cathode-electrolyte interface (Fig. 5f), indicating the average rate of WGSR is positive. From the above analysis, it can be seen that the reversible WGSR can contribute significantly to CO production at a low operating potential but it can consume CO at a high operating potential.

4. Conclusions

An electrochemical model is developed to characterize the performance of an SOEC used for H_2O/CO_2 co-electrolysis. The model is validated by comparing the simulation results with experimental data from the literature.

It is found that the rate of WGSR in the porous cathode can be positive or negative, depending on the temperature and local gas composition. A new method is proposed to quantify the contribution of reversible WGSR to CO production, by comparing the CO fluxes at the cathode-electrolyte interface and at the cathode surface. It is also found that reversible WGSR

can produce CO or consume CO, depending on the average rate of WGSR in the porous cathode. In the simulated case at an operating temperature of 873, the reversible WGSR contributes to about 25% of CO production, while at 1073K, the reversible WGSR consumes about 19% of CO produced from CO_2 electrolysis. In addition, the gas composition at the cathode surface greatly influences the distribution of WGSR rate inside the cathode. Large negative rate of WGSR is observed near the cathode surface with very low molar fraction of CO. Generally, the WGSR plays an important role in CO production at a low operating potential while the WGSR can consume CO at high operating potential.

The present study provides detailed information for better understanding the working mechanism of SOEC used for H_2O/CO_2 co-electrolysis. The new method proposed is useful to quantify the contributions of WGSR and CO_2 electrolysis to CO production. The electrochemical model can be integrated into 2D/3D model for more detailed analysis and simulation.

Acknowledgement:

This research was supported by a grant (No. A-PK48) from The Hong Kong Polytechnic University, Hong Kong.

References:

[1] M. Ni, M.K.H. Leung, D.Y.C. Leung, K. Sumathy, Renewable Sustainable Energy Rev. 11(2007) 401-425.
[2] M. Ni, D.Y.C. Leung, M.K.H. Leung, K. Sumathy, Fuel Process Technol. 87 (2006) 461-472.
[3] A. Steinfeld, Solar Energy 78(2005) 603-615.
[4] M. Fishcher, Int. J. Hydrogen Energy 11 (1986) 495-501.
[5] M. Ni, M.K.H. Leung, D.Y.C. Leung, Int. J. Hydrogen Energy 33(2008) 2337-2354.
[6] S. Fujiwara, S. Kasai, H. Yamauchi, K. Yamada, S. Makino, K. Matsunaga, M. Yoshino, T. Kameda, T. Ogawa, S. Momma, E. Hoashi, Prog. Nucl. Energy 50(2008) 422-426.
[7] A. Brisse, J. Schefold, M. Zahid, Int. J. Hydrogen Energy 33 (2008) 5375-5382.
[8] Y. Bo, Z. Wenqiang, X. Jingming, C. Jing, Int. J. Hydrogen Energy 33(2008) 6873-6877.
[9] M. Liang, B. Yu, M. Wen, J. Chen, J. Xu, Y. Zhai, J. Power Sources 190 (2009) 341-345.
[10] M.A. Laguna-Bercero, S.J. Skinner, J.A. Kilner, J. Power Sources 192 (2009) 126-131.
[11] M.A. Laguna-Bercero, R. Campana, A. Larrea, J.A. Kilner, V.M. Orera, J. Power Sources 196 (2011) 8942-8947.
[12] J. Schefold, A. Brisse, M. Zahid, J. Electrochem. Soc. 156(2009) B897-B904.
[13] S. Kim, J. Yu, D. Seo, I. Han, S. Woo, ECS Trans. 35(2011) 2957-2960.
[14] J.J. Hartvigsen, S. Elangovan, J.E. O'Brien, C.M. Stoots, J.S. Herring, ECS Trans. 7(2007) 357-363.
[15] R. Knibbe, M.L. Traulsen, A. Hauch, S.D. Ebbesen, M. Mogensen, J. Electrochem. Soc. 157(2010) B1209-B1217.
[16] N.Q. Minh, ECS Trans. 35(2011) 2897 – 2904.
[17] A. Hauch, S.D. Ebbesen, S.H. Jensen, M. Mogensen, J. Electrochem. Soc. 155 (2008) B1184 – B1193.
[18] M.A. Laguna-Bercero, R. Campana, A. Larrea, J.A. Kilner, V.M. Orera, J. Electrochem. Soc. 157(2010) B852-B855.
[19] J.E. O'Brien, C.M. Stoots, J.S. Herring, P.A. Lessing, J.J. Hartvigsen, S. Elangovan, J. Fuel Cell Sci. Technol. 2 (2005) 156- 163.
[20] J.E. O'Brien, C.M. Stoots, J.S. Herring, J. Hartvigsen, J. Fuel Cell Sci. Technol. 3 (2006) 213 – 219.
[21] F. Chauveau, J. Mougin, F. Mauvy, J. Bassat, J. Grenier, Int. J. Hydrogen Energy 36 (2011) 7785-7790.
[22] Q. Liu, C. Yang, X. Dong. F.L. Chen, Int. J. Hydrogen Energy 35(2010) 10039-10044.
[23] P.K. Patro, T. Delahaye, E. Bouyer, P.K. Sinha, Int. J. Hydrogen Energy, in press.
[24] D. Grondin, J. Deseure, P. Ozil, J.P. Chabriat, B. Grondin-Perez, A. Brisse, Computing approach of cathodic process within solid oxide electrolysis cell: experiments and continuum model validation, J. Power Sources, in press.
[25] J. Udagawa, P. Aguiar, N.P. Brandon, J. Power Sources 166 (2007) 127-136.
[26] J. Udagawa, P. Aguiar, N.P. Brandon, J. Power Sources 180 (2008) 354-364.
[27] J. Udagawa, P. Aguiar, N.P. Brandon, J. Power Sources 180 (2008) 46-55.
[28] J. Laurencin, D. Kane, G. Delette, J. Deseure, F. Lefebvre-Joud, J. Power Sources 196 (2011) 2080-2093.
[29] M. Ni, M.K.H. Leung, D.Y.C. Leung, Int. J. Hydrogen Energy 32 (2007) 2305-2313.
[30] M. Ni, M.K.H. Leung, D.Y.C. Leung, Electrochim. Acta 52 (2007) 6707 – 6718.
[31] M. Ni, Int. J. Hydrogen Energy 34 (2009) 7795-7806.

[32] G. Hawkes, J.O'Brien, C. Stoots, B. Hawkes, Int. J. Hydrogen Energy 34 (2009) 4189-4197.
[33] E.A. Harvego, M.G. Mckellar, J.E. O'Brien, J.S. Herring, Nucl. Eng. Des. 239(2009) 1571-1580.
[34] S.D. Ebbesen, J. Hogh, K.A. Nielsen, J.U. Nielsen, M. Mogensen, Int. J. Hydrogen Energy 36(2011) 7363-7373.
[35] S.H. Jensen, X. Sun, S.D. Ebbesen, R. Knibbe, M. Mogensen, Int. J. Hydrogen Energy 35 (2010) 9544-9549.
[36] Z.L. Zhan, W. Kobsiriphat, J.R. Wilson, J. Pillai, I. Kim, S.A. Barnett, Energy & Fuels 23 (2009) 3089 – 3096.
[37] Z.L. Zhan, L. Zhao, Electrochemical reduction of CO_2 in solid oxide electrolysis cells, Journal Power Sources, in press.
[38] C.M. Stoots, J.E. O'Brien, J.S. Herring, J.J. Hartvigsen, J. Fuel Cell Sci. Technol. 6 (2009) 011014.
[39] J.E. O'Brien, M.G. Mckellar, C.M. Stoots, J.S. Herring, G.L. Hawkes, Int. J. Hydrogen Energy 34 (2009) 4216-4226.
[40] S.D. Ebbesen, C. Graves, M. Mogensen, Int. J. Green Energy 6(2009) 646-660.
[41] S.D. Ebbesen, M. Mogensen, J. Power Sources 193 (2009) 349-358.
[42] K.R. Sridhar, B.T. Vaniman, Solid State Ionics 93 (1997) 321- 328.
[43] G. Tao, K.R. Sridhar, C.L. Chan, Solid State Ionics 175 (2004) 615-619.
[44] G. Tao, K.R. Sridhar, C.L. Chan, Solid State Ionics 175 (2004) 621-624.
[45] C. Graves, S.D. Ebbesen, M. Mogensen, Solid State Ionics 192 (2011) 398-403.
[46] M. Ni, Chem. Eng. J. 164 (2010) 246-254.
[47] M.W. Chase, NIST-JANAF Thermochemical Tables, 4th ed., American Chemical Society, American Institute of Physics for the National Institute of Standards and Technology, 1998.
[48] Y. Vural, L. Ma, D.B. Ingham, M. Pourkashanian, J. Power Sources 195 (2010) 4893-4904.
[49] R. Suwanwarangkul, E. Croiset, M.W. Fowler, P.L. Douglas, E. Entchev, M.A. Douglas, J. Power Sources 122 (2003) 9-18.
[50] M. Ni, D.Y.C. Leung, M.K.H. Leung, J. Power Sources 183 (2008) 668 – 673.
[51] R.C. Reid, J.M. Prausnitz, B.E. Poling, The Properties of Gases & Liquids, 4th Edition, McGraw-Hill Book Company, New York, 1987.
[52] B.A. Haberman, J.B. Young, Int. J. Heat Mass Transfer 47(2004) 3617 – 3629.
[53] R. Suwanwarangkul, E. Croiset, E Entchev, S Charojrochkul, M.D. Pritzker, M.W. Fowler, P.L. Douglas, S Chewathanakup, H Mahaudom, J. Power Sources 161(2006) 308-322.
[54] M.M. Hussain, X Li, I Dincer, Int. J. Energy Research 29(2005) 1083-1101.
[55] J.L. Yuan, B Sunden, J. Fuel Cell Sci. Technol. 3(2006) 89-98.
[56] R.A. Gemmen, J Trembly, J. Power Sources 161(2006) 1084-1095.
[57] V Verda, M.R. Von Spakovsky, J. Fuel Cell Sci. Technol. 6(2009) 011005-1 - 011005-9.
[58] I Zinovik, D Poulikakos, Electrochim. Acta 54(2009) 6234 – 6243.
[59] H Iwai, Y Yamamoto, M Saito, H Yoshida, Energy 36(2011) 2225-2234.
[60] Personal communication with Dr. M. S. Sohal from Idaho National Laboratory, at ASME 2010 8th International Fuel Cell Science, Engineering & Technology Conference, June 14–16, 2010, Brooklyn, New York, USA.
[61] H.Y. Zhu, R.J. Kee, J. Power Source 117(2003) 61-74.
[62] E. Hernandez-Pacheco, M.D. Mann, P.N. Hutton, D. Singh and K.E. Martin, Int J Hydrogen Energy **30** (2005) 1221–1233.
[63] P. Costamagna, A. Selimovic, M.D. Borghi and G. Agnew, Chem Eng J **102** (2004) 61–69.

[64] S.H. Chan and Z.T. Xia, J Appl Electrochem **32** (2002) 339–347.
[65] Y. Matsuzaki and I. Yasuda, J. Electrochem. Soc. **147** (2000) 1630–1635.
[66] A.M. Sukeshini, B. Habibzadeh, B.P. Becker, C.A. Stoltz, B.W. Eichhorn and G.S. Jackson, J. Electrochem. Soc. **153** (2006) A705–A715.
[67] M. Ni, M.K.H. Leung and D.Y.C. Leung, Energy Convers. Manage.**48** (2007) 1525–1535.
[68] W. Lehnert, J. Meusinger and F. Thom, J. Power Sources **87** (2000) 57–63.

List of Tables

1. Parameters used in calculating the effective diffusion coefficients [51]

2. Parameters used in parametric simulations

List of Figures

1. Working mechanisms of SOEC for co-electrolysis of H_2O and CO_2

2. Comparison of calculated data with experimental data by Zhan et al' [36] for model validation

3. Effect of temperature on co-electrolysis of H_2O and CO_2 in an SOEC at an operating potential of 1.3V and inlet gas composition (molar fraction) of H_2O: 49.7%; H_2: 25%; CO_2: (25%); and CO (0.3%) – (a) Rate of reversible WGSR; (b) Molar fraction of H_2O and H_2; (c) Molar fraction of CO_2 and CO; (d) Current density; (e) Flux ($mol.m^{-2}.s^{-1}$) of CO and H_2 at 873K; (f) Flux ($mol.m^{-2}.s^{-1}$) of CO and H_2 at 1073K;

4. Effect of gas composition at the cathode surface, at an operating temperature of 1073K and an operating potential of 1.3V – (a) Rate of reversibleWGSR; (b) Distributions of gas molar fraction at an inlet gas composition (molar fraction) of H_2O: 49.7%; CO_2: 25%; CO: 25%; and H_2: 0.3%; (c) Distributions of gas molar fraction at an inlet gas composition (molar fraction) of H_2O: 25%; CO_2: 49.7%; H_2: 25%; and CO: 0.3%; (d) Current density; (e) Flux ($mol.m^{-2}.s^{-1}$) of CO and H_2 at cathode surface gas composition of H_2O: 49.7%, CO_2: 25%, H_2: 25%, CO: 0.3%; (f) Flux ($mol.m^{-2}.s^{-1}$) of CO and H_2 at cathode surface gas composition of H_2O: 25%, CO_2: 49.7%, H_2: 25%, CO: 0.3%;

5. Effect of operating potential at an operating temperature of 1073K and inlet gas composition (molar fraction) of H_2O: 49.7%, CO_2: 25%, H_2: 25%, CO: 0.3% – (a) Rate of reversibleWGSR; (b) Molar fraction of H_2O and H_2; (c) Molar fraction of CO_2 and CO; (d) Current density; (e) Flux ($mol.m^{-2}.s^{-1}$) of CO and H_2 at an operating potential of 1.0V; (f) Flux ($mol.m^{-2}.s^{-1}$) of CO and H_2 at an operating potential of 1.4V;

Table 1. Parameters used in calculating the effective diffusion coefficients [51]

	CO	CO_2	H_2	O_2	N_2	H_2O
σ_i	3.69	3.941	2.827	3.467	3.798	2.641
ε_i / k	91.7	195.2	59.7	106.7	71.4	809.1

Table 2. Parameters used in the simulation

Parameter	Value
Operating temperature, T (K)	1073
Operating pressure, P (atm)	1.0
Electrode porosity, ε	0.4
Electrode tortuosity, ξ	2.0
Average pore radius, r_p (μm)	0.5
Cathode-supported SOEC:	
Anode thickness d_a (μm)	50
Electrolyte thickness, L (μm)	50
Cathode thickness, d_c (μm)	500
Anode inlet gas molar ratio: O_2/N_2	0.21/0.79
Cathode inlet gas molar ratio*: $H_2O/CO_2/H_2/CO$	0.497/0.25/0.25/0.03
SOEC operating potential (V)	1.3

* Various gas compositions are studied and the details can be found from the text.

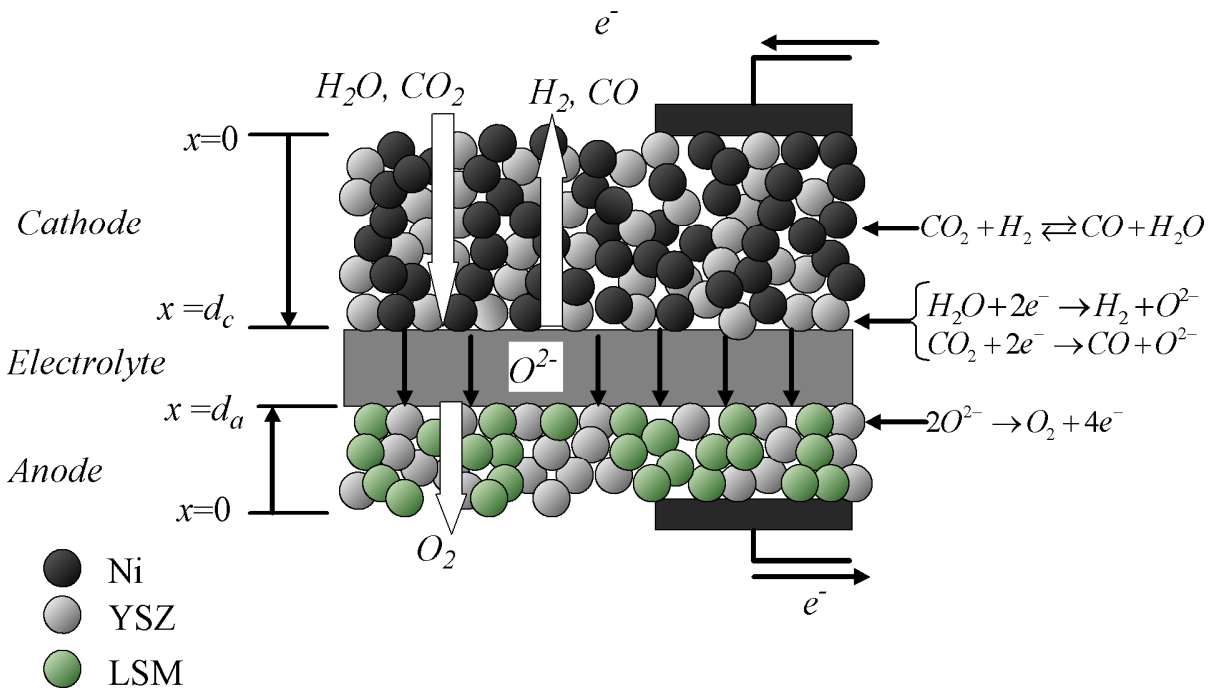
e-
H2O, CO2
H2, CO
x=0
Cathode
x =dc
Electrolyte
x =da
Anode
x=0
O2-
O2
e-
CO2 + H2 ⇄ CO + H2O
H2O + 2e− → H2 + O2−
CO2 + 2e− → CO + O2−
2O2− → O2 + 4e−
Ni
YSZ
LSM

Fig. 1.

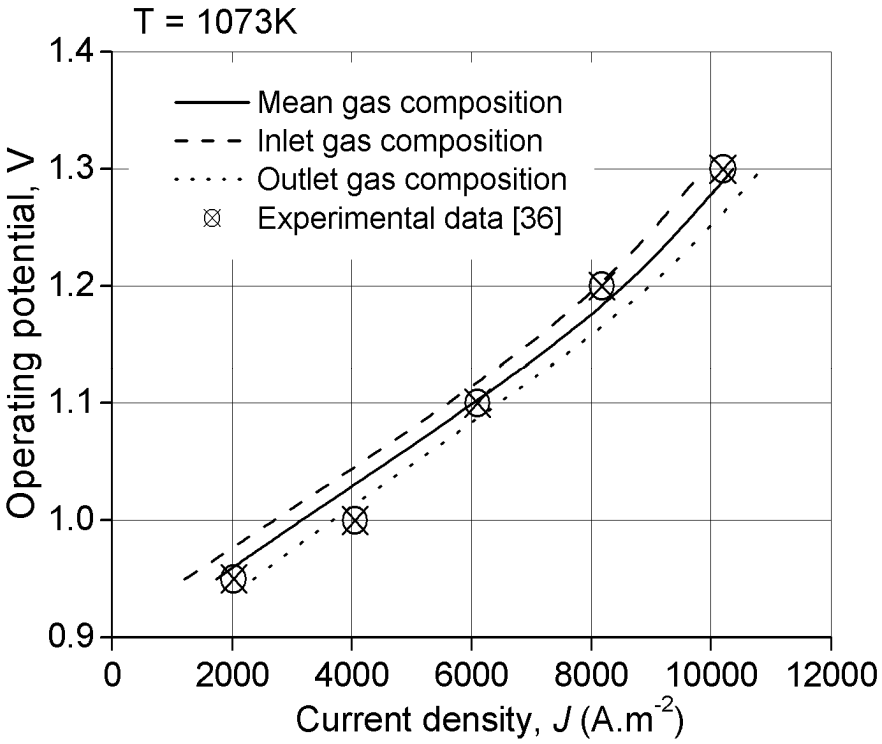
T = 1073K
Mean gas composition
Inlet gas composition
Outlet gas composition
Experimental data [36]
Operating potential, V
Current density, J (A.m-2)
1.4
1.3
1.2
1.1
1.0
0.9
0
2000
4000
6000
8000
10000
12000

Fig. 2.

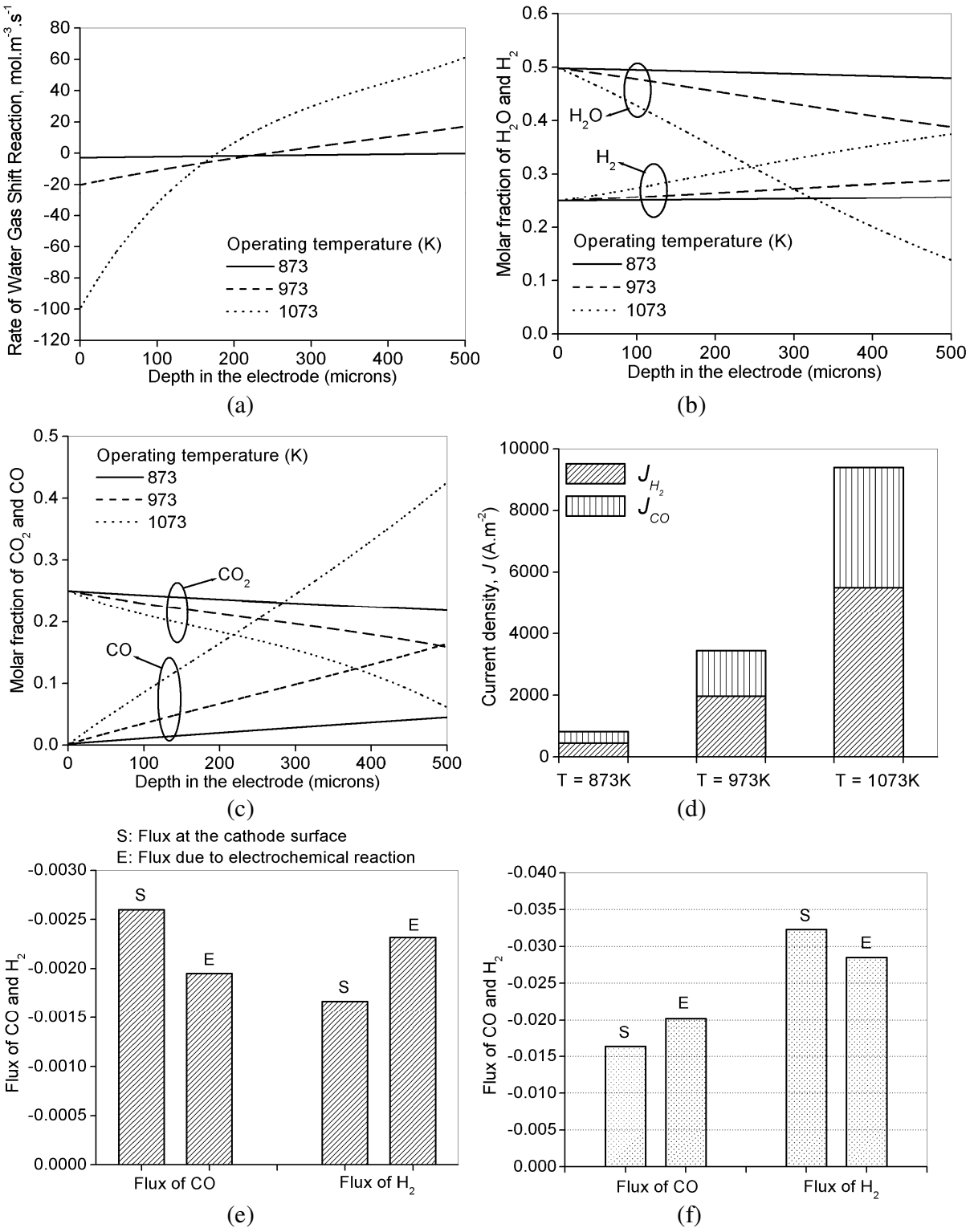
Rate of Water Gas Shift Reaction, mol.m-3.s-1
Depth in the electrode (microns)
Operating temperature (K)
873
973
1073
(a)
Molar fraction of H2O and H2
H2O
H2
Depth in the electrode (microns)
(b)
Molar fraction of CO2 and CO
CO2
CO
(c)
Current density, J (A.m-2)
JH2
JCO
T = 873K
T = 973K
T = 1073K
(d)
S: Flux at the cathode surface
E: Flux due to electrochemical reaction
Flux of CO and H2
Flux of CO
Flux of H2
(e)
(f)

Fig. 3.

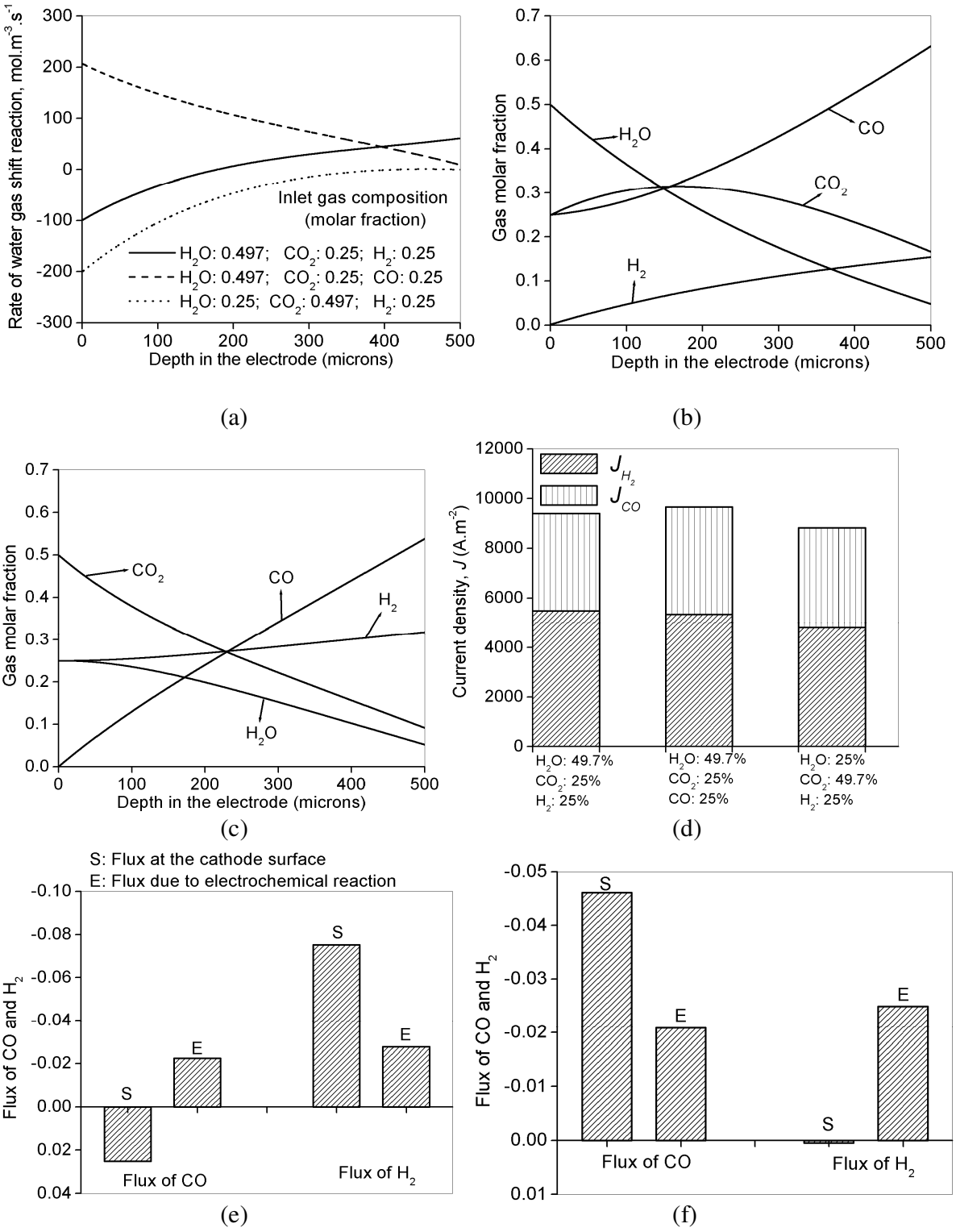
Rate of water gas shift reaction, mol.m-3.s-1
Depth in the electrode (microns)
Inlet gas composition
(molar fraction)
H2O: 0.497; CO2: 0.25; H2: 0.25
H2O: 0.497; CO2: 0.25; CO: 0.25
H2O: 0.25; CO2: 0.497; H2: 0.25
(a)
Gas molar fraction
Depth in the electrode (microns)
H2O
CO
CO2
H2
(b)
Gas molar fraction
Depth in the electrode (microns)
CO2
CO
H2
H2O
(c)
Current density, J (A.m-2)
JH2
JCO
H2O: 49.7%
CO2: 25%
H2: 25%
H2O: 49.7%
CO2: 25%
CO: 25%
H2O: 25%
CO2: 49.7%
H2: 25%
(d)
S: Flux at the cathode surface
E: Flux due to electrochemical reaction
Flux of CO and H2
S
E
S
E
Flux of CO
Flux of H2
(e)
Flux of CO and H2
S
E
S
E
Flux of CO
Flux of H2
(f)

Fig. 4.

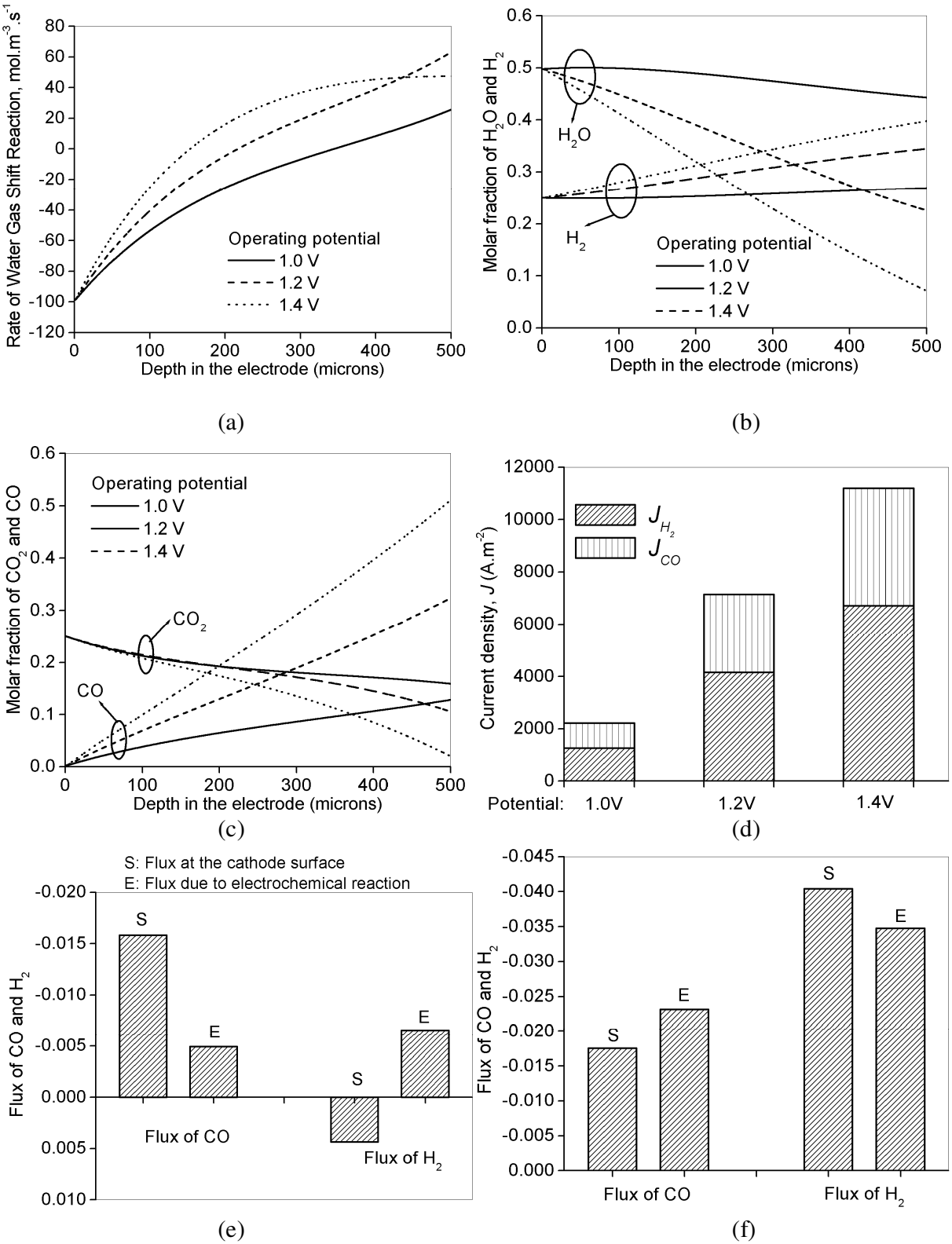
Rate of Water Gas Shift Reaction, mol.m-3.s-1
Depth in the electrode (microns)
Operating potential
1.0 V
1.2 V
1.4 V
(a)
Molar fraction of H2O and H2
H2O
H2
Depth in the electrode (microns)
Operating potential
1.0 V
1.2 V
1.4 V
(b)
Molar fraction of CO2 and CO
CO2
CO
Depth in the electrode (microns)
Operating potential
1.0 V
1.2 V
1.4 V
(c)
Current density, J (A.m-2)
JH2
JCO
Potential: 1.0V 1.2V 1.4V
(d)
S: Flux at the cathode surface
E: Flux due to electrochemical reaction
Flux of CO and H2
S
E
S
E
Flux of CO
Flux of H2
(e)
Flux of CO and H2
S
E
S
E
Flux of CO
Flux of H2
(f)

Fig. 5.